

Bismuth layer properties in the ultrathin Bi–FeNi multilayer films probed by spectroscopic ellipsometry

N. N. Kovaleva,^{1,*} D. Chvostova,² O. Pacheroova,² A. V. Muratov,¹
L. Fekete,² I. A. Sherstnev,¹ K. I. Kugel,^{3,4} F. A. Pudonin,¹ and A. Dejneka²

¹*Lebedev Physical Institute, Russian Academy of Sciences, Leninsky prospect 53, 119991 Moscow, Russia*

²*Institute of Physics, Academy of Sciences of the Czech Republic, Na Slovance 2, 18221 Prague, Czech Republic*

³*Institute for Theoretical and Applied Electrodynamics,
Russian Academy of Sciences, 125412 Moscow, Russia*

⁴*National Research University Higher School of Economics, 101000 Moscow, Russia*

(Dated: January 13, 2023)

Using wide-band (0.5–6.5 eV) spectroscopic ellipsometry we study ultrathin [Bi(0.6–2.5 nm)–FeNi(0.8,1.2 nm)]_N multilayer films grown by rf sputtering deposition, where the FeNi layer has a nanoisland structure and its morphology and magnetic properties change with decreasing the nominal layer thickness. From the multilayer model simulations of the ellipsometric angles, $\Psi(\omega)$ and $\Delta(\omega)$, the complex (pseudo)dielectric function spectra of the Bi layer were extracted. The obtained results demonstrate that the Bi layer can possess the surface metallic conductivity, which is strongly affected by the morphology and magnetic properties of the nanoisland FeNi layer in the GMR-type Bi–FeNi multilayer structures.

The spin-orbit coupling (SOC) is a relativistic effect important for the electronic structure of heavy atoms and solids formed by them. This leads to characteristic surface metallic states arising from the loss of the inversion symmetry at the surface (Rashba effect) [1]. Bismuth (Bi) is a rather heavy element with strong SOC in the atomic $6p$ levels (where $p_{3/2} - p_{1/2}$ splitting is about 1.5 eV), which facilitates the application of quasi-two-dimensional (2D) Bi layers in spintronics as spin sources or filters, as well as in multilayer structures exhibiting the giant magnetoresistance (GMR) effect. The scaling of Bi integrated units to smaller dimensions is still going on toward the thickness of 5 nm and beyond, where 2D Bi (bismuthene) exhibits extraordinary electronic properties [2]. For implementing the full potential of GMR applications by a rational nanostructure design, the information on the electron band structure of 2D Bi layers is important.

In bulk Bi, which crystallizes in the rhombohedral symmetry (space group $R\bar{3}m$, unit cell parameters $a = b = 4.547 \text{ \AA}$, $c = 11.8616 \text{ \AA}$, $\alpha = \beta = 90^\circ$, $\gamma = 120^\circ$) with two atoms per unit cell, five bands accommodate ten valence electrons, which dictates an insulating behavior generically. However, the bands close to the Fermi level, namely, at the T and L points of the Brillouin zone, can be significantly affected by the strong SOC [3]. As a consequence, three conduction minima at the L points lie at about 40 meV lower than the single valence-band maximum at the T point. This indirect band overlap implies the semimetallic behavior of bulk Bi with electron transport properties dictated by quite small electron effective mass along a certain axis and unusually long mean free path. Due to the crystal structure inversion symmetry,

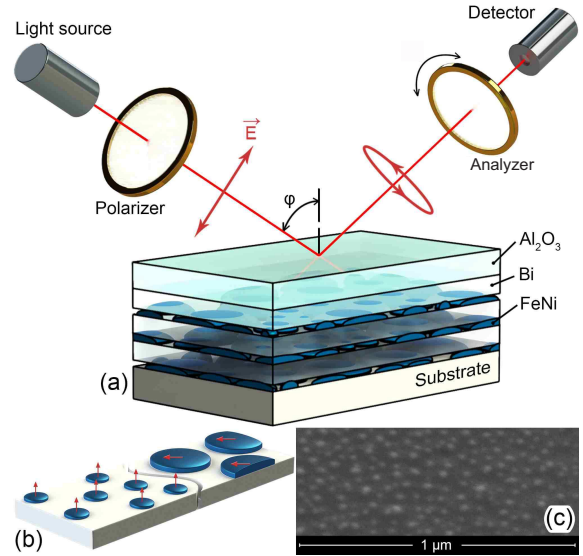


FIG. 1: Schematics of (a) the ultrathin [Bi–FeNi]_N multilayer films investigated in the present study by spectroscopic ellipsometry and (b) the magnetization configuration in the nanoisland FeNi layer. Larger islands exhibit an in-plane magnetization configuration, while smaller islands can have an out-of-plane one [9, 14] (for more details, see the text). (c) SEM image of the nanoisland FeNi layer on the Si(111) substrate obtained by using a JEOL JSM-7001F facility. Reproduced with permission from Phys. Lett. A 410, 127546 (2021) [13]. Copyright 2021. Elsevier.

the SOC does not lead to any lifting of the spin degeneracy in the $6p$ bands, each having two possible spin states per k point in the Brillouin zone, while the loss of symmetry at the surface or interface can transform Bi from a semimetal (SM) to a metal when the electron or hole bands cross the Fermi level.

In the thin-film limit, this effect can be at conflict with the quantum confinement effect (or size-effect), leading

*Electronic address: kovalevann@lebedev.ru

to complicated electronic properties. Quantum effects can be observed in thin films whose thickness is comparable to the effective wavelength of charge carriers, and their mean free path exceeds the film thickness. These conditions should transform Bi from a SM to a semiconductor (SC) at a critical film thickness of about 300 \AA [4]. Due to a very low charge carrier density ranging from about 10^{17} cm^{-3} to 10^{18} cm^{-3} and small relative effective masses of the charge carriers from 0.005 to 0.1, the optical excitation of charge carriers starts to be relevant only in the far infrared (below 0.1 eV) [5], where a confinement-induced energy gap in thin Bi films could manifest itself in the optical experiments. However, the surface metallic states may hinder the SM-SC transition in ultrathin Bi films. The existence of the surface metallic states in ultrathin Bi(001) films was confirmed by the broadband terahertz time-domain spectroscopy study [6]. It was shown that the surface charge carrier density, plasma frequency, and scattering rate dramatically increase with a decrease in the film thickness, reaching $n = 3.1 \times 10^{19} \text{ cm}^{-3}$, $\omega_p = 4.0 \times 10^2 \text{ THz}$ (1.65 eV), and $\gamma_D = 4.8 \times 10^2 \text{ THz}$ (2.0 eV), respectively, in the thinnest investigated 2.8 nm Bi film [6], where the estimated optical conductivity dc limit $\sigma_{1(\omega \rightarrow 0)} = \omega_p^2 / \gamma_D = 2300 \Omega^{-1} \cdot \text{cm}^{-1}$.

Recently, we have demonstrated that the electronic properties of the free and localized Ta charge carriers in $(\text{Ta-FeNi})_N$ multilayer films (MLFs) can be studied by spectroscopic ellipsometry (SE) [7, 8]. Here, we explore the elaborated SE approach to gain insights into the electron band structure and surface electronic properties of ultrathin Bi layers in real GMR-type $(\text{Bi-FeNi})_N$ MLF structures, incorporating nanoisland FeNi layers (see the scheme of the $(\text{Bi-FeNi})_N$ MLFs investigated in the present study by SE in Fig. 1(a)). The morphology and magnetic properties of a single-layer nanoisland FeNi film grown on the Sitall substrate were studied earlier [9–11]. Below the structural percolation transition at the nominal thickness of 1.5–1.8 nm [12], the FeNi layer is discontinuous and consists of inhomogeneously distributed FM nanoislands having lateral sizes of 5–30 nm and possessing giant magnetic moments of 10^3 – $10^5 \mu_B$ (where μ_B is the Bohr magneton). As an example, Fig. 1(c) shows the scanning electron microscopy (SEM) image of the nanoisland FeNi film grown on the Sitall substrate [13]. As schematically shown in Fig. 1(b), the larger islands (which appear closer to the percolation transition) have the in-plane magnetization configuration, while the smaller islands (existing quite far from the percolation transition) have the out-of-plane one [9, 14]. Here, collective superferromagnetic (SFM) states – FM or AFM – may develop in the self-assembled local arrangements of FM nanoislands at comparatively high temperatures [9, 15]. However, small and well separated FeNi nanoislands are weakly interacting via the magnetic dipole forces and exhibit superparamagnetic (SPM) behavior at high temperatures, which is associated with strongly fluctuating giant magnetic moments [9].

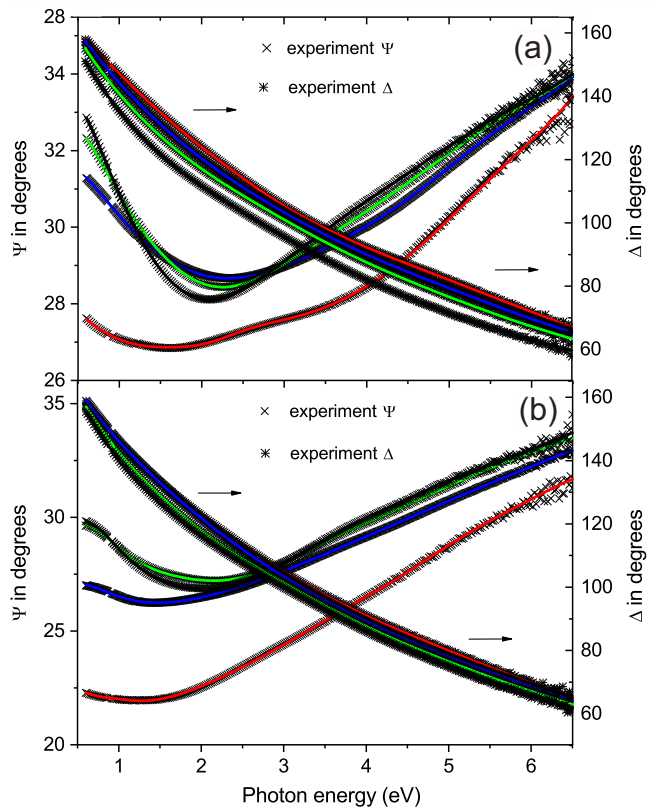


FIG. 2: Ellipsometric angles, $\Psi(\omega)$ and $\Delta(\omega)$, measured for the $\text{Al}_2\text{O}_3(2.1 \text{ nm})/[\text{Bi-FeNi}(h)]_{16}/\text{Sitall}$ MLF samples having the FeNi layer thickness h (a) 1.2 nm and (b) 0.8 nm at an angle of incidence of 70° (symbols) and the fitting results by the Drude-Lorentz model (Eq. (1)) (displayed for the Bi layer thickness of 2.5, 2.0, 1.4, and 0.6 nm by solid black, green, blue, and red curves, respectively).

The $(\text{Bi-FeNi})_N$ MLFs were grown by rf sputtering deposition from 99.95 % pure Bi and $\text{Fe}_{21}\text{Ni}_{79}$ targets on glass Sitall (TiO_2) substrates. Before the deposition, the vacuum chamber was annealed at 200°C , so that the prepared base pressure in the chamber was below 2×10^{-6} Torr. During the deposition, the background Ar pressure was 6×10^{-4} Torr. The actual temperature of the substrates was about 80°C . We used the Sitall substrates with typical sizes of $15 \times 5 \times 0.6 \text{ mm}^3$. The Bi and FeNi layer nominal thickness was controlled by the deposition time determined by the film deposition rate. For example, the determined FeNi layer deposition rate was about 0.67 \AA per second. To protect the grown MLFs from the oxidation under ambient conditions, the as deposited MLFs were covered *in situ* by the 2.1 nm-thick Al_2O_3 layer. In the prepared $(\text{Bi-FeNi})_N$ MLF samples, the FeNi layer nominal thickness was 0.8 and 1.2 nm, the thickness of the Bi layer was 0.6, 1.4, 2.0, and 2.5 nm, and the number of Bi/FeNi bilayers was $N = 16$. In our recent study, (Ta-FeNi) MLFs grown by rf sputtering deposition onto Sitall-glass substrates, including ultrathin 0.52 nm-thick FeNi layers, were characterized by scanning/transmission electron microscopy (STEM) (for details see [8]). Here, the grown Bi-FeNi MLF samples were

TABLE I: Parameters of the Drude and low-energy Lorentz bands for the Bi layer in the MLFs [Bi(2.5, 2.0, 1.4 nm)–FeNi(0.8, 1.2 nm)]₁₆, resulting from the model simulations of the complex dielectric response (Eq. (1)) (for details see supplementary material).

FeNi (nm)	Bi (nm)	A_D	γ_D (eV)	A_j	E_j (eV)	γ_j (eV)
1.2	2.5	25±4	1.4±0.1	96±18	0.32	0.83
	2.0	23±3	2.2±0.1	97±9	0.40	1.08
	1.4	64±0.3	0.75±0.17	19±9	0.81	1.32
0.8	2.5			97±1	0.459	1.271
	2.0			98±1	0.481	1.354
	1.4			103±1	0.429	1.628

characterized by the atomic-force microscopy (AFM), X-ray diffraction, and X-ray reflectivity (see supplementary material to this article). The X-ray reflectivity measurements confirm a good periodicity and relatively small interface roughness in the grown Bi–FeNi MLF structures, as well as good agreement with the nominal thickness of the Bi and FeNi layers. The X-ray diffraction suggests orientation of the Bi layers along the (012) plane, where the interlayer distance is 3.28 Å. Thus, the prepared Bi–FeNi MLFs having the Bi layer thickness of 0.6, 1.4, 2.0, and 2.5 nm correspond to about 2, 4, 6, and 8 Bi(012) monolayers. The ellipsometric angles $\Psi(\omega)$ and $\Delta(\omega)$ were measured for the prepared Al₂O₃/(Bi–FeNi)₁₆/Si₁₁₁ MLF samples at room temperature at three or four angles of incidence of 60°, 65°, 70°, and 75° in a wide photon energy range of 0.5–6.5 eV with a J.A. Woollam VUV-VASE spectroscopic ellipsometer (Fig. 2(a,b) illustrates the $\Psi(\omega)$ and $\Delta(\omega)$ measured at 70°). The complex dielectric function $\tilde{\epsilon}(\omega) = \epsilon_1(\omega) + i\epsilon_2(\omega)$ of each Bi or FeNi layer was modeled by the Drude term and the sum of Lorentz oscillators to account for the contributions of free charge carriers and interband optical transitions, respectively

$$\tilde{\epsilon}(E \equiv \hbar\omega) = \epsilon_\infty - \frac{A_D}{E^2 + iE\gamma_D} + \sum_j \frac{A_j\gamma_j E_j}{E_j^2 - E^2 - iE\gamma_j}, \quad (1)$$

where ϵ_∞ is the high frequency dielectric constant. The fitted Drude parameters were A_D (related to the plasma frequency ω_p via $A_D = \epsilon_\infty \hbar\omega_p^2$) and scattering rate γ_D . The adjustable Lorentz oscillator parameters were E_j , γ_j , and A_j of the peak energy, full width at half maximum, and ϵ_2 peak height, respectively. The ellipsometric angles, $\Psi(\omega)$ and $\Delta(\omega)$, measured at different angles of incidence were fitted simultaneously in the framework of the multilayer model Al₂O₃/[Bi(2.5, 2.0, 1.4, 0.6 nm)–FeNi(0.8, 1.2 nm)]₁₆/Si₁₁₁, where, in addition, the surface roughness was taken into account by the standard effective medium approximation (EMA) based on the Bruggeman model (50% Al₂O₃ – 50% vacuum), using the J.A. Woollam VASE software [16]. In the simulation of the ellipsometric angles, $\Psi(\omega)$ and $\Delta(\omega)$, the Bi layers in each MLF structure were described by the disper-

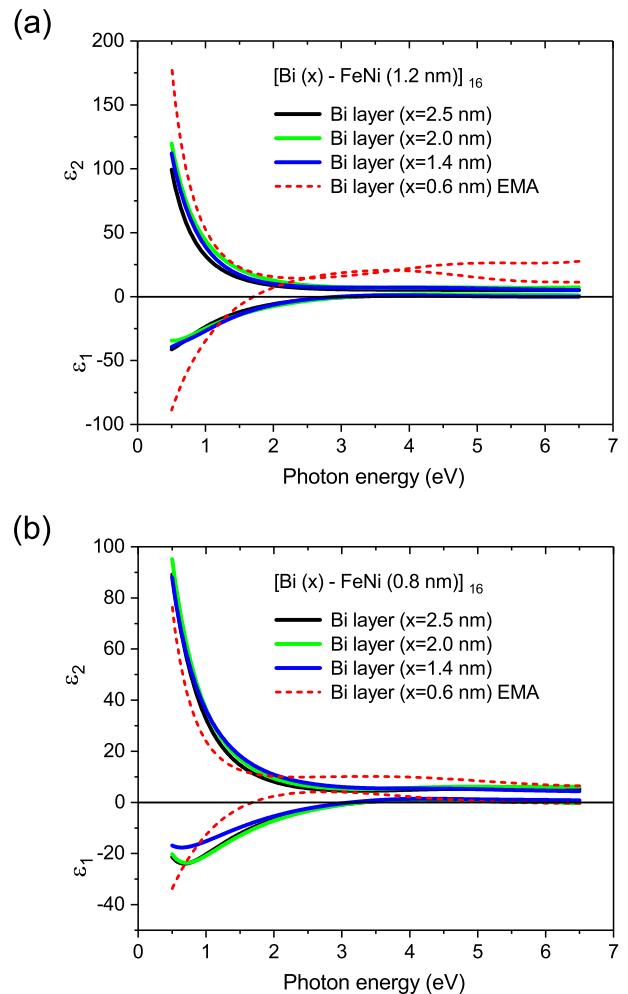


FIG. 3: The complex dielectric function spectra, $\epsilon_2(\omega)$ and $\epsilon_1(\omega)$, of the Bi layer in the [Bi(2.5, 2.0, 1.4, 0.6 nm)–FeNi(h)]₁₆ MLFs for the FeNi layer thickness h (a) 1.2 nm and (b) 0.8 nm are shown by solid black, green, blue, and dashed red curves, respectively.

sion models (Eq. (1)), including three Lorentz oscillators and the Drude term where necessary. The discontinuous nanoisland FeNi layers were modeled by the effective dielectric function in EMA, which describes the optical properties of a complex composite by an effective homogeneous medium. In the utilized multilayer model, the spectra of the complex dielectric function of the blank Si₁₁₁ substrate obtained from our previous SE studies [17, 18] were substituted. The Bi and FeNi layer thicknesses were fitted to their respective nominal values. The good quality of the fit obtained for the measured angle of incidence of 70° is demonstrated by Fig. 2(a,b), where we plot the recorded ellipsometric angles $\Psi(\omega)$ and $\Delta(\omega)$ and the fitting results. The details of the used model and the resulting Drude-Lorentz parameters along with the fit quality check are given in supplementary material to this article. The simulation in the framework of the multilayer model for the Al₂O₃/(Bi–FeNi)₁₆/Si₁₁₁ MLFs, where the Bi–FeNi interface roughness is explicitly included, does not essentially improve the fit (see the

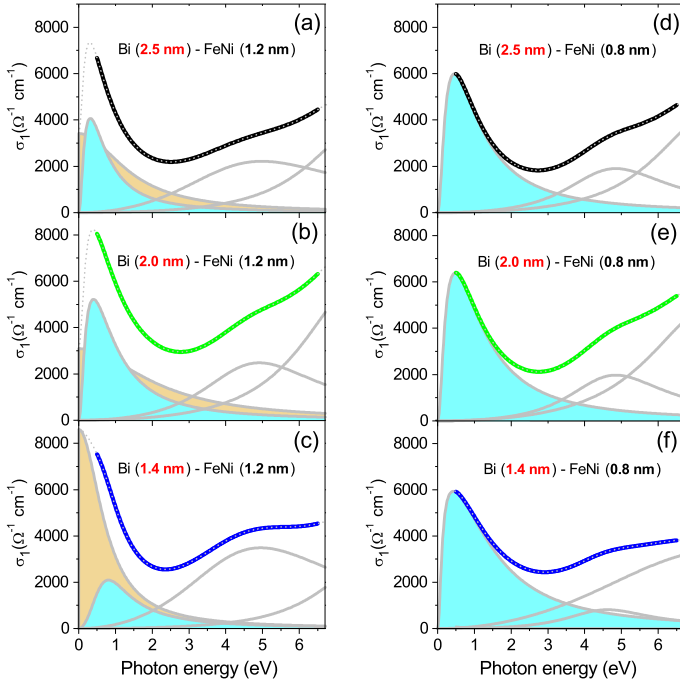


FIG. 4: The Bi intralayer optical conductivity, $\sigma_1(\omega) = \varepsilon_2(\omega)\omega[\text{cm}^{-1}]/60$, in the $[\text{Bi}-\text{FeNi}(h)]_{16}$ MLFs shown by solid black, green, and blue curves, for the FeNi layer thickness h (a–c) 1.2 nm and (d–f) 0.8 nm, respectively. The contributions from the low-energy Lorentz oscillator and the Drude term are indicated by the cyan and yellow shaded area, respectively. The summary contribution of the Drude and Lorentz bands is shown by dotted lines.

analysis presented in [7]), suggesting that the Bi–FeNi interface roughness is essentially incorporated in the EMA dielectric function of the nanoisland FeNi layers.

From the multilayer model simulations, the dielectric function spectra of the Bi and FeNi layers were obtained (see supplementary material for details). Here, we are particularly interested in the dielectric function spectra, $\varepsilon_1(\omega)$ and $\varepsilon_2(\omega)$, of the Bi layer in the studied $[\text{Bi}(2.5, 2.0, 1.4, 0.6 \text{ nm})-\text{FeNi}(1.2 \text{ nm})]_{16}$ and $[\text{Bi}(2.5, 2.0, 1.4, 0.6 \text{ nm})-\text{FeNi}(0.8 \text{ nm})]_{16}$ MLFs, and the spectra obtained from the best-fit simulations of the $\Psi(\omega)$ and $\Delta(\omega)$ are shown in Fig. 3(a,b). One can notice different trends in the behavior of the corresponding $\varepsilon_1(\omega)$ and $\varepsilon_2(\omega)$ spectra. Thus, the $\varepsilon_1(\omega)$ spectra in Fig. 3(b) exhibit a clearly pronounced minimum at about 0.8 eV, whereas $\varepsilon_1(\omega)$ spectra in Fig. 3(a) display more negative values falling down to -50 . Accordingly, the $\varepsilon_2(\omega)$ spectra in Fig. 3(a) demonstrate a steeper rise at the lowest probed photon energies. Moreover, the dielectric function spectra of the 0.6 nm-thick Bi layers in the studied $[\text{Bi}(0.6 \text{ nm})-\text{FeNi}(0.8, 1.2 \text{ nm})]_{16}$ MLFs display apparent trends toward more pronounced metallic behavior at the lowest probed photon energies, the $\varepsilon_1(\omega)$ exhibits a sharp downturn to negative values, and $\varepsilon_2(\omega)$ dramatically increases (see Fig. 3(a,b) and supplementary material to this article).

In Fig. 4(a–f) we present the Bi intralayer optical

conductivity, $\sigma_1(\omega) = \varepsilon_2(\omega)\omega[\text{cm}^{-1}]/60$, in the studied $[\text{Bi}(2.5, 2.0, 1.4 \text{ nm})-\text{FeNi}(0.8, 1.2 \text{ nm})]_{16}$ MLFs. Here, the dispersion analysis representation resulting from the multilayer model simulations using Eq. (1) is explicitly demonstrated. On one hand, the simulation results for the three $[\text{Bi}(2.5, 2.0, 1.4 \text{ nm})-\text{FeNi}(0.8 \text{ nm})]_{16}$ MLF structures, including the 0.8 nm-thick nanoisland FeNi layer, indicate that the Bi layer low-energy response is dominated by a pronounced Lorentz band peaking at 0.43–0.48 eV having the ε_2 peak height of 97–103 (see Table I). The low-energy interband transition with a high oscillator strength is observed in the dense Bi layers at the energy of 0.8 eV having the ε_2 peak height of about 120 [19, 20]. The low-energy peak at 0.8 eV is also seen in the averaged over anisotropy low-energy dielectric function response of single crystals [21, 22]. This strong low-energy optical transition is associated with interband transitions with the onset near the Γ point, $\Gamma_6^+ - \Gamma_6^-$ and $\Gamma_{45}^+ - \Gamma_6^-$ [23], and with interband transitions near the T point $T_6^- - T_{45}^-$ [24]. Therefore, we can conclude that the low-energy optical response of the Bi layer in the $[\text{Bi}(2.5, 2.0, 1.4 \text{ nm})-\text{FeNi}(0.8 \text{ nm})]_{16}$ MLFs (see Fig. 4(d–f)) is dominated by the Bi semimetallic-like electron band structure. On the other hand, our model simulations imply that the optical conductivity of the Bi layer in the $[\text{Bi}(2.5, 2.0, 1.4 \text{ nm})-\text{FeNi}(1.2 \text{ nm})]_{16}$ MLFs, including the 1.2 nm-thick nanoisland FeNi layer, has competing contributions from the low-energy Lorentz band and from the Drude term (see Fig. 4(a–c) and Table I). For the 2.5 and 2.0 nm thick Bi layers, the estimated Drude parameters are similar to those characterizing the surface metallic states arising due to the Rashba effect in ultrathin Bi(001) films [6] ($\sigma_{1(\omega \rightarrow 0)} = 2300 \Omega^{-1} \cdot \text{cm}^{-1}$ and $\gamma_D = 2.0 \text{ eV}$). However, it was shown that the surface layer in the ultrathin Bi(012) films can possess a pseudocubic Bi{012}-oriented allotrope with the even number of layers (represented by black phosphorus-like puckered layers) [25]. We have found that with decreasing the Bi layer thickness from 2.0 to 1.4 nm (corresponding to about six and four Bi(012) monolayers, respectively), the Drude dc limit $\sigma_{1(\omega \rightarrow 0)}$ significantly increases from about 3100 ± 400 to $8600 \pm 40 \Omega^{-1} \cdot \text{cm}^{-1}$, and the scattering rate γ_D decreases from 2.2 ± 0.2 to $0.8 \pm 0.2 \text{ eV}$. At the same time, the low-energy Lorentz band becomes significantly suppressed (see Fig. 4(a–c)). The observed evolution of the competing Drude and Lorentz parts can be attributed to the progressive increase in the contribution of the Bi surface metallic states. However, note the difference from the results obtained for the 40–2.8 nm-thick Bi(001) single-layer films [6], where the ω_p and γ_D increase with a decrease of the film thickness. We suppose that here a GMR-like case plays an important role. Indeed, in the GMR-type MLF structures, FM coupling is found for 2.5 nm and 1.3 nm-thick spacer layers, and AFM coupling is found for a 2 nm-thick spacer layer [26]. The existence of AFM or FM GMR-type correlations between the discontinuous nanoisland FeNi layers could occur in the SFM regime [9, 11, 15]. Therefore, in the

studied GMR-type [Bi(2.5, 2.0, 1.4 nm)–FeNi(1.2 nm)]₁₆ MLFs, the magnetic interaction between the neighboring FeNi layers, which is responsible for the spin-dependent scattering in the magnetic layer, oscillates from FM via AFM to FM ones. The spin-dependent scattering at the Bi/FeNi interface necessarily affects the scattering of the Bi surface metallic charge carriers (γ_D), which should decrease for the FM coupling and increase for the AFM coupling between the neighboring FeNi layers. The decrease of the γ_D of the surface metallic charge carriers in the FM regime will naturally lead to the increase in the optical *dc* conductivity limit (see Fig. 4(c)). According to the results of the present multilayer model simulations for the [Bi(2.5, 2.0, 1.4 nm)–FeNi(0.8, nm)]₁₆ MLFs, including the 0.8 nm-thick nanoisland FeNi layers, the Bi layer exhibits semimetallic bulk-like electron band structure, however, the Drude surface metallic conductivity (the Drude term) is implicit in Fig. 4(d–f). Here, with decreasing the FeNi layer thickness, strong SPM-type fluctuations of giant magnetic moments of the FeNi nanoislands become important [9, 11]. In our recent study [8], we reported that this leads to localization phenomena in the GMR-type MLFs, introduced by an additional strong magnetic disorder and long-range many-body interactions between giant magnetic moments of FeNi nanoislands. Therefore, the lack of evidence on the surface metallic states for the Bi layer in the [Bi(2.5, 2.0, 1.4 nm)–FeNi(0.8, nm)]₁₆ MLFs can be referred to strong SPM-type fluctuations of giant magnetic moments of FM FeNi nanoislands, leading to strong scattering and localization of scarce free charge carriers in the Bi surface layer. In addition, we found that the dielectric function spectra of the two Bi{012} monolayers demonstrate pronounced metallicity properties in the [Bi(0.6 nm)–FeNi(0.8, 1.2 nm)]₁₆ MLFs. The origin of the discovered semimetal-to-metal crossover needs to be further investigated. In particular, the impact of lattice mismatch at the interface on

the electron band structure of 2D bismuthene [2] and the AFM mechanism of a giant SOC-splitting [27] in the presence of AFM spin textures at the interface should be considered.

In conclusion, using the advances of the spectroscopic ellipsometry approach, we extracted the (pseudo)dielectric function spectra of the ultrathin Bi layers incorporating from two to eight Bi(012) monolayers in the [Bi(0.6, 1.4, 2.0, 2.5, nm)–FeNi(0.8, 1.2 nm)] multilayer structures grown by rf sputtering deposition. We found that the Bi(012) layers inside the studied multilayer film structures can possess the surface metallic conductivity, which is strongly influenced by the morphology and magnetic properties of the nanoisland FeNi layer. The obtained results may be useful for implementing the full potential of the GMR applications based on quasi-2D Bi layers.

See the supplementary material for the atomic force microscopy (AFM), X-ray reflectivity (XRR), and X-ray diffraction (XRD) characterization of the MLFs and for details of the spectroscopic ellipsometry study.

This work was partially supported by the Czech Science Foundation (Project No. 20-21864S), and European Structural and Investment Funds and the Czech Ministry of Education, Youth, and Sports (Project No. SOLID21, CZ.02.1.01/0.0/0.0/16_019/0000760). The theoretical analysis performed by K. Kugel was supported by the Russian Science Foundation, project No. 21-12-0254 (<https://rscf.ru/en/project/21-12-00254/>).

The authors have no conflicts to disclose.

The data that support the findings of this study are available within this article (and its supplementary material).

-
- [1] Y. A. Bychkov and E. I. Rashba, *JETP Lett.* **39**, 78 (1984).
- [2] M.-Y. Liu, Y. Huang, Q.-Y. Chen, Z.-Y. Li, C. Cao, and Y. He, *RSC Adv.* **7**, 39546 (2017).
- [3] X. Gonze, J.-P. Michenaud, and J.-P. Vigneron, *Phys. Rev. B* **41**, 11827 (1990).
- [4] C. A. Hoffman, J. R. Meyer, F. J. Bartoli, A. Di Venere, X. J. Yi, C. L. Hou, H. C. Wang, J. B. Ketterson, and G. K. Wong, *Phys. Rev. B* **48**, 11431 (1993).
- [5] J. Toudert, R. Serna, I. Camps, J. Wojcik, P. Mascher, E. Rebollar, and T. A. Ezquerra, *J. Phys. Chem. C* **121**, 3511 (2017).
- [6] K. Yokota, J. Takeda, C. Dang, G. Han, D. N. McCarthy, T. Nagao, S. Hishita, K. Kitajima, and I. Katayama, *Appl. Phys. Lett.* **100**, 251605 (2012).
- [7] N. N. Kovaleva, D. Chvostova, O. Pacherova, L. Fekete, K. I. Kugel, F. A. Pudonin, and A. Dejneka, *Appl. Phys. Lett.* **111**, 183104 (2017).
- [8] N. N. Kovaleva, F. V. Kusmartsev, A. B. Mekhiya, I. N. Trunkin, D. Chvostova, A. B. Davydov, L. N. Oveshnikov, O. Pacherova, I. A. Sherstnev, A. Kusmartseva, K. I. Kugel, A. Dejneka, F. A. Pudonin, Y. Luo, and B. A. Aronzon, *Sci. Rep.* **10**, 21172 (2020).
- [9] A. Stupakov, A. V. Bagdinov, V. V. Prokhorov, A. N. Bagdinova, E. I. Demikhov, A. Dejneka, K. I. Kugel, A. A. Gorbatshevich, F. A. Pudonin, and N. N. Kovaleva, *J. Nanomater.*, 3190260 (2016).
- [10] A. P. Boltaev, F. A. Pudonin, I. A. Sherstnev, and D. A. Egorov, *J. Phys. Condens. Matter* **30**, 295804 (2018).
- [11] N. N. Kovaleva, A. V. Bagdinov, A. Stupakov, A. Dejneka, E. I. Demikhov, A. A. Gorbatshevich, F. A. Pudonin, K. I. Kugel, and F. V. Kusmartsev, *J. Nanopart. Res.* **20**, 109 (2018).
- [12] A. P. Boltaev, F. A. Pudonin, I. A. Sherstnev, and D. A. Egorov, *J. Exp. Theor. Phys.* **125**, 465 (2017).
- [13] D. D. Noskova, F. A. Pudonin, I. A. Sherstnev, G. N. Eroshenko, D. A. Egorov, and A. M. Shadrin, *Phys. Lett. A* **410**, 127546 (2021).

- [14] E. Y. Vedmedenko, H. P. Oepen, and J. Kirschner, Phys. Rev. B **67**, 012409 (2003).
- [15] W. Kleemann, O. Petravic, Ch. Binek, G. N. Kakazei, Yu. G. Pogorelov, J. B. Sousa, S. Cardoso, and P. P. Freitas, Phys. Rev. B **63**, 134423 (2001).
- [16] J.A. Woollam *VASE Spectroscopic Ellipsometry Data Analysis Software*. (J.A. Woollam Co.: Lincoln, NE, USA, 2010).
- [17] N. Kovaleva, D. Chvostova, and A. Dejneka, Metals **7**, 257 (2017).
- [18] N. N. Kovaleva, D. Chvostova, A. V. Bagdinov, M. G. Petrova, E. I. Demikhov, F. A. Pudonin, and A. Dejneka, Appl. Phys. Lett. **106**, 051907 (2015).
- [19] O. Hunderi, J. Phys. F **5**, 2214 (1975).
- [20] J. Toudert and R. Serna, Opt. Mater. Express **7**, 2299 (2017).
- [21] P. Y. Wang and A. L. Jain, Phys. Rev. B **2**, 2978 (1970).
- [22] A. P. Lenham, D. M. Treherne, and R. J. Metcalfe, J. Opt. Soc. Am. **55**, 1072 (1965).
- [23] S. Golin, Phys. Rev. B **166**, 643 (1968).
- [24] Y. Liu and R. Allen, Phys. Rev. B **52**, 1566 (1995).
- [25] T. Nagao, J. T. Sadowski, M. Saito, S. Yaginuma, Y. Fujikawa, T. Kogure, T. Ohno, Y. Hasegawa, S. Hasegawa, and T. Sakurai, Phys. Rev. Lett. **93**, 105501 (2004).
- [26] A. Hütten, S. Mrozek, S. Heitmann, T. Hempel, H. Brückl, and G. Reiss, Acta Mater. **47**, 4245 (1999).
- [27] L.-D. Yuan, Z. Wang, J.-W. Luo, E. I. Rashba, and A. Zunger, Phys. Rev. B **102**, 014422 (2020).